1   T-dependent B cell responses to *Plasmodium* induce antibodies that form

2   a high-avidity multivalent complex with the circumsporozoite protein

3

4   Short Title: Antibody responses to the *Plasmodium* circumsporozoite protein

5

6   Camilla R. Fisher[1][¶], Henry J. Sutton[2][¶], Joe A. Kaczmarski[1], Hayley A. McNamara[2],

7   Ben Clifton[1], Joshua Mitchell[1], Yeping Cai[2], Johanna N. Dups[2], Nicholas J. D'Arcy[2],

8   Mandeep Singh[2], Aaron Chuah[2], Thomas S. Peat[3], Colin J. Jackson[1]* and Ian A.

9   Cockburn[2]*

10

11   1. Research School of Chemistry, The Australian National University, Canberra, ACT

12   2601, Australia

13

14   2. John Curtin School of Medical Research, The Australian National University,

15   Canberra, ACT 2601, Australia

16

17   3. CSIRO Biomedical Manufacturing Program, Parkville, VIC 3052, Australia

18

19   * Corresponding authors

20   E-mail: colin.jackson@anu.edu.au

21   E-mail: ian.cockburn@anu.edu.au (lead contact).

22

23   [¶] These authors contributed equally to this work

24

25

26 **Abstract**

27

28   The repeat region of the *Plasmodium falciparum* circumsporozoite protein (CSP) is a

29   major vaccine antigen because it can be targeted by parasite neutralizing antibodies;

30   however, little is known about this interaction. We used isothermal titration

31   calorimetry, X-ray crystallography and mutagenesis-validated modeling to analyze

32   the binding of a murine neutralizing antibody to *Plasmodium falciparum* CSP.

33   Strikingly, we found that the repeat region of CSP is bound by multiple antibodies.

34   This repeating pattern allows multiple weak interactions of single F_{AB} domains to

35   accumulate and yield a complex with a dissociation constant in the low nM range.

36   Because the CSP protein can potentially cross-link multiple B cell receptors (BCRs)

37   we hypothesized that the B cell response might be T cell independent. However,

38   while there was a modest response in mice deficient in T cell help, the bulk of the

39   response was T cell dependent. By sequencing the BCRs of CSP-repeat specific B

40   cells in inbred mice we found that these cells underwent somatic hypermutation and

41   affinity maturation indicative of a T-dependent response. Last, we found that the BCR

42   repertoire of responding B cells was limited suggesting that the structural simplicity

43   of the repeat may limit the breadth of the immune response.

44

45

46   **Author Summary**

47

48   Vaccines aim to protect by inducing the immune system to make molecules called

49   antibodies that can recognize molecules on the surface of invading pathogens. In the

50   case of malaria, our most advanced vaccine candidates aim to promote the production

51   of antibodies that recognize the circumsporozoite protein (CSP) molecule on the

52   surface of the invasive parasite stage called the sporozoite. In this report we use X-ray

53   crystallography to determine the structure of CSP-binding antibodies at the atomic

54   level. We use other techniques such as isothermal titration calorimetry and structural

55   modeling to examine how this antibody interacts with the CSP molecule. Strikingly,

56   we found that each CSP molecule could bind 6 antibodies. This finding has

57   implications for the immune response and may explain why high titers of antibody are

58   needed for protection. Moreover, because the structure of the CSP repeat is quite

59   simple we determined that the number of different kinds of antibodies that could bind

60   this molecule are quite small. However a high avidity interaction between those

61   antibodies and CSP can result from a process called affinity maturation that allows the

62   body to learn how to make improved antibodies specific for pathogen molecules.

63   These data show that while it is challenging for the immune system to recognize and

64   neutralize CSP, it should be possible to generate viable vaccines targeting this

65   molecule.

66

3

Introduction

67

68

69   Malaria caused by *Plasmodium falciparum* causes the deaths of around

70   430,000 people each year [1]. The most advanced vaccine candidate for malaria is the

71   RTS,S/AS01 vaccine which consists of a truncated version of the sporozoite-surface

72   circumsporozoite protein (CSP), packaged in a Hepatitis C core virus-like particle

73   delivered in AS01 - a proprietary liposome based adjuvant [2]. Phase II and Phase III

74   clinical trials have repeatedly demonstrated that the vaccine gives around 50%

75   protection against clinical malaria in field settings for the first year following

76   vaccination [3]. The bulk of protection is attributed to antibodies targeting the CSP

77   repeat epitope included within the vaccine, with some contribution from CD4+ T cells

78   [4]. It is still unclear why the antibody response to CSP is only partially protective.

79   We lack structural information about how neutralizing antibodies bind to CSP and

80   knowledge on the breadth and nature of the B cell response elicited.

81

82   Antibodies to CSP were first identified as potential mediators of protection

83   following seminal studies that showed that immunization with irradiated sporozoites

84   could induce sterile protection against live parasite challenge [5,6]. In the early 1980s,

85   monoclonal antibodies (mAbs) isolated from mice immunized with sporozoites were

86   found to be capable of blocking invasion of hepatocytes [7] and directly neutralizing

87   parasites by precipitating the surface protein coat (a process known as the

88   circumsporozoite reaction) [8]. These antibodies were then used to clone CSP, one of

89   the first malaria antigens identified [8,9]. The N- and C-terminal domains of CSP

90   from all *Plasmodium* species are separated by a repeat region, which was the target of

91   the original mAbs [9-11]. In the 3D7 reference strain of *P. falciparum,* the CSP repeat

4

92   has 38 asparagine-alanine-asparagine-proline (NANP)-repeats interspersed with 4

93   asparagine-valine-aspartate-proline (NVDP) repeats that are concentrated towards the

94   N-terminus [12] though different isolates can contain slightly different numbers of

95   repeats [13]. One of the most effective *P. falciparum* sporozoite neutralizing

96   antibodies identified in these early studies was 2A10 which can block sporozoite

97   infectivity *in vitro* [7] and in *in vivo* mouse models utilizing rodent *P. berghei*

98   parasites expressing the *P. falciparum* CSP repeat region [14,15].

99

100   While CSP binding antibodies have been shown to be able to neutralize

101   sporozoites and block infection, it has also been proposed that CSP is an

102   immunological "decoy" that induces a suboptimal, but broad, T-independent immune

103   response due to the CSP repeat cross-linking multiple B cell receptors (BCRs) [16].

104   However, it remains unknown if the repetitive regions of CSP can cross-link multiple

105   BCRs as they are not as large as typical type-II T-independent antigens [17].

106   Moreover, the ability to induce a T-independent response does not preclude a T-

107   dependent component to immunity as well: various oligomeric viral surface proteins

108   can induce both short-lived T-independent responses and subsequent affinity matured

109   IgG responses [18,19]. Furthermore, the very little published data on the sequences of

110   CSP binding antibodies does not convincingly support activation of a broad B cell

111   repertoire: a small study of five *P. falciparum* CSP mouse monoclonal antibodies

112   (mAbs) identified some shared sequences [20]. In humans, a study that generated

113   mAbs from three individuals who received RTS,S found that the three antibodies

114   studied had distinct sequences though these all used similar heavy chains [21].

115

116   We therefore set out to test the hypothesis that the CSP repeat can bind

117   multiple antibodies or BCRs and drive a T-independent immune response. To do this

118   we undertook a comprehensive biophysical characterization of the 2A10 sporozoite-

119   neutralizing antibody that binds to the CSP repeat. We found that this antibody binds

120   with an avidity in the nano-molar range which was unexpected as previous studies

121   using competition ELISAs with peptides predicted a micro-molar affinity [22,23].

122   Strikingly, isothermal titration calorimetry (ITC), structural analyses, and

123   mutagenesis-validated modeling revealed that the CSP repeat can be bound by around

124   six antibodies suggesting that the repeat may potentially crosslink multiple BCRs on

125   the surface of a B cell. However, analysis of CSP-specific B cells revealed that CSP-

126   specific B cells can enter Germinal Centers (GCs) and undergo affinity maturation

127   contradicting the notion that the response to CSP is largely T-independent. Moreover,

128   we found that the BCR repertoire of CSP-binding B cells is quite limited which may

129   restrict the size and effectiveness of the immune response.

130   **Results**

131

132   **Characterization of the thermodynamics of 2A10-antigen binding**

133

134   We began our analysis by performing isothermal titration calorimetry (ITC) to

135   understand the interaction between 2A10 and CSP. For ease of expression we used a

136   recombinant CSP (rCSP) construct described previously which was slightly truncated

137   with 27 repeats [24]. ITC experiments were run on the purified 2A10 antibody and the

138   purified 2A10 antigen-binding fragment (F_{AB}) fragment to test the thermodynamic

139   basis of the affinity of 2A10 F_{AB} towards CSP. Experiments were also performed on

140   the 2A10 F_{AB} fragment with the synthetic peptide antigen $(NANP)_6$, which is a short

141   segment of the antigenic NANP-repeat region of CSP (**Table 1; Fig. 1**). The binding

142   free energies (ΔG) and dissociation constants (K_D) were found to be -49.0 kJ/mol and

143   2.7 nM for the full 2A10 antibody with CSP, -40 kJ/mol and 94 nM for the 2A10 F_{AB}

144   with CSP, and -36.4 kJ/mol and 420 nM for the 2A10 F_{AB} with the $(NANP)_6$ peptide.

145   Surprisingly, we did not observe a typical 1:1 antibody/F_{AB} domain:antigen

146   binding stoichiometry (Table 1). We found that each $(NANP)_6$ peptide was bound to

147   by ~2 F_{AB} fragments (2.8 repeats per F_{AB} domain). With the rCSP protein we

148   observed that ~11 F_{AB} fragments could bind to each rCSP molecule, (2.5 repeats per

149   F_{AB} domain. Finally, when the single-domain F_{AB} fragment is replaced by the full

150   2A10 antibody (which has two F_{AB} domains), we observe binding of 5.8 antibodies

151   per rCSP molecule (4.7 repeats per antibody). Therefore all complexes exhibit

152   approximately the same binding stoichiometry of two F_{AB} fragments/domains per ~5

153   repeat units. These results suggest that the antigenic region of CSP constitutes a

154   multivalent antigen and that repeating, essentially identical, epitopes must be

155   available for the binding of multiple F_{AB} domains.

156   **Table 1. Thermodynamic parameters for interactions between 2A10 F_{AB}, 2A10**

157   **and antigens.**

	$(NANP)_6$:F_{AB}	rCSP:F_{AB}	rCSP:2A10
K_a (M^{-1})	$(2.37 \pm 0.91) \times 10^6$	$(1.07 \pm 0.39) \times 10^7$	$(3.6 \pm 2.7) \times 10^8$
K_d (nM)	420 ± 160	94 ± 34	2.7 ± 2.1
ΔH (kJ/mol complex)	-113 ± 5	-1245 ± 112	-1175 ± 44
TΔS (kJ/mol complex)	-76.6 ± 4.9	-1205 ± 112	-1126 ± 44
ΔG (kJ/mol complex)	-36.4 ± 1.0	-40.0 ± 0.9	-49.0 ± 1.9
n (F_{AB}/2A10: Ag)	2.16 ± 0.06	10.8 ± 0.7	5.8 ± 0.1

158   Parameters were determined by ITC at 25 °C. Errors for n (Ag : F_{AB}), K_a and

159   ΔH (complex) are 95% confidence intervals estimated from a single titration; errors

160   for other parameters were propagated.

161   It is not possible to separate affinity from avidity in this system, although it is

162   apparent that there is a substantial benefit to the overall strength of binding between

163   the antibody and antigen through the binding of multiple F_{AB} domains. The F_{AB}:rCSP

164   complex and the 2A10:rCSP complex had similar enthalpy and entropy of binding

165   (**Table 1**), but the 2A10:rCSP complex had a lower overall ΔG binding,

166   corresponding to a lower dissociation constant (2.7 nM *vs.* 94 nM for F_{AB}:rCSP). The

167   observation that this antibody-antigen (Ab-Ag) interaction is primarily enthalpically

168   driven is consistent with the general mechanism of Ab-Ag interactions [25]. It is clear

169   that the dissociation constant (K_d) of a single F_{AB} domain to the $(NANP)_6$ peptide is

170   substantially higher (420 nM), and that the avidity, the accumulated strength of the

171   multiple binding events between the F_{AB} domains of the antibody and the CSP repeat,

172   is the basis for the lower K_d value observed in the 2A10:rCSP complex. Thus, the

173   characteristic repeating pattern of the epitope on the CSP antigen allows multiple

174   weak interactions with 2A10 F_{AB} domains to accumulate, which yields a complex

175   with a high avidity dissociation constant in the low nM range.

176

177   **Structural analysis of the (NANP)-repeat region and the 2A10 F_{AB}**

178

179   To better understand the molecular basis of the multivalent interaction

180   between 2A10 and rCSP, we performed structural analysis of the components.

181   Previous work indicated that the NANP-repeat region of CSP adopts a flexible rod-

182   like structure with a regular repeating helical motif that provides significant

183   separation between the N-terminal and the C-terminal domains [26]. Here, we

184   performed far-UV circular dichroism (CD) spectroscopy to investigate the structure of

185   the (NANP)$_6$ peptide. These results were inconsistent with a disordered random coil

186   structure (**S1 Fig**.). Rather, the absorption maximum around 185 nm, minimum

187   around 202 nm and shoulder between 215 and 240 nm, is characteristic of intrinsically

188   disordered proteins that can adopt a spectrum of states [27].

189

190   The lowest energy structures of the (NANP)$_6$ repeat were predicted using the

191   PEP-FOLD *de novo* peptide structure prediction algorithm [28]. The only extended

192   state among the lowest energy structures that was consistent with the reported spacing

193   of the N-and C-terminal domains of CSP [26], and which presented multiple

194   structurally similar epitopes was a linear, quasi-helical structure, which formed a

195   regularly repeating arrangement of proline turns (**Fig. 2A**). The theoretical CD

196   spectrum of this conformation was calculated (**S1 Fig.**), qualitatively matching the

197   experimental spectra: the maximum was at 188 nm, the minimum at 203 nm and there

198   was a broad shoulder between 215 and 240 nm. To investigate the stability of this

199   conformation, we performed a molecular dynamics (MD) simulation on this peptide,

200   which showed that this helical structure could unfold, and refold, on timescales of

201   tens of nanoseconds, supporting the idea that it is a low-energy, frequently sampled,

202   configuration in solution (**S1 Mov.**, **S2 Fig**.). We also observed the same

203   characteristic hydrogen bonds between a carbonyl following the proline and the amide

204   nitrogen of the alanine, and the carbonyl group of an asparagine and a backbone

205   amide of asparagine three residues earlier, that are observed in the crystal structure of

206   the NPNA fragment [29]. Thus, this configuration, which is consistent with

207   previously published experimental data, is a regular, repeating, extended

208   conformation that would allow binding of multiple F_{AB} domains to several

209   structurally similar epitopes.

210

211   To better understand the interaction between the 2A10 and the (NANP)-repeat

212   region, we solved the crystal structure of the 2A10 F_{AB} fragment in two conditions (**S1**

213   **Table**), yielding structures that diffracted to 2.5 Å and 3.0 Å. All of the polypeptide

214   chains were modeled in good quality electron density maps (**Fig. 2B**), except for

215   residues 134-137 of the light chain. This loop is located at the opposite end of the F_{AB}

216   fragment to the variable region and not directly relevant to antigen binding. The 2.5 Å

217   structure contained a single polypeptide in the asymmetric unit, whereas the 3.0 Å

218   structure contained three essentially identical chains. Superposition of the four unique

219   F_{AB} fragments from the two structures revealed that the variable antigen binding

220   region is structurally homogeneous, suggesting that this region might be relatively

221   pre-organized in the 2A10 F_{AB}. This is consistent with the observation that antibodies

222   typically undergo relatively limited conformational change upon epitope binding [25].

223   Indeed, a recent survey of 49 Ab-Ag complexes revealed that within the binding site,

10

224   the heavy chain Complementarity Determining Region (CDR)-3 was the only element

225   that showed significant conformational change upon antigen binding and even this

226   was only observed in one third of the antibodies [30].

227

228   Attempts to obtain a crystal structure of a complex between 2A10 F_{AB} and the

229   (NANP)$_6$ peptide were unsuccessful; unlike binary Ab-Ag interactions, in which the

230   Ab will bind to a single epitope on an antigen and produce a population of structurally

231   homogeneous complexes that can be crystallized, in this interaction we are dealing

232   with an intrinsically-disordered peptide, the presence of multiple binding sites on the

233   peptide, and the possibility that more than one 2A10 F_{AB} domain can bind the peptide.

234   Therefore it is difficult to obtain a homogeneous population of complexes, which is a

235   prerequisite for crystallization. Attempts to soak the (NANP)$_6$ peptide into the high-

236   solvent form of 2A10 F_{AB}, in which there were no crystal packing interactions with

237   the binding-loops, caused the crystals to dissolve, again suggesting that the

238   heterogeneity of the peptide and the presence of multiple epitopes produces disorder

239   that is incompatible with crystal formation.

240

241   **Modeling the interaction of the 2A10 F_{AB} with the NANP-repeat region and**

242   **testing the model through site-directed mutagenesis**

243

244   Although it was not possible to obtain a crystal structure of the 2A10-

245   (NANP)$_6$ peptide complex, the accurate structures of the 2A10 F_{AB} fragment, the

246   (NANP)$_6$ peptide, and the knowledge that antibodies seldom undergo significant

247   conformational changes upon antigen binding [30], allowed us to model the

248   interaction, which we tested using site directed mutagenesis. Computational modeling

11

249   of Ab-Ag interactions has advanced considerably in recent years and several

250   examples of complexes with close to atomic accuracy have been reported in the

251   literature [31]. Using the SnugDock protein-protein docking algorithm [31], we

252   obtained an initial model for binding of the peptide to the CDR region of the 2A10

253   F_{AB} fragment (**Fig. 2C**). We then performed, in triplicate, three 50 ns MD simulations

254   on this complex to investigate whether the interaction was stable over such a time

255   period (**S2 Mov.**, **S3 Fig.**). These simulations confirmed that the binding mode that

256   was modeled is stable, suggesting that it is a reasonable approximation of the

257   interaction between these molecules. To experimentally verify whether our model of

258   the 2A10 F_{AB}:(NANP)$_6$ peptide interaction was plausible, we performed site directed

259   mutagenesis of residues predicted to be important for binding. Our model predicted

260   that the interaction with (NANP)$_6$ would be mainly between CDR2 and CDR3 of the

261   light chain and CDR2 and CDR3 of the heavy chain (**Fig. 2C**).

262

263   In the light chain (**Fig. 3A,B**), Y38 is predicted to be one of the most

264   important residues in the interaction; it contributes to the formation of a hydrophobic

265   pocket that buries a proline residue and is within hydrogen bonding distance, *via* its

266   hydroxyl group, to a number of backbone and side-chain groups of the peptide. Loss

267   of this side-chain abolished binding. Y56 also forms part of the same proline-binding

268   pocket as Y38, and loss of this side-chain also resulted in an almost complete loss of

269   binding. R109 forms a hydrogen bond to an asparagine residue on the side of the

270   helix; mutation of this residue to alanine results in a partial loss of binding. Y116 is

271   located at the center of the second proline-binding pocket; since loss of the entire

272   side-chain through an alanine mutation would lead to general structural disruption of

273   the F_{AB} fragment, we mutated this to a phenylalanine (removing the hydroxyl group),

12

274   which led to a significant reduction in binding. Finally, S36A was selected as a

275   control: the model indicated that it was outside the binding site, and the ELISA data

276   indicated that had no effect on $(NANP)_n$ binding.

277

278   Within the heavy chain (**Fig. 3C,D**), mutation of N57 to alanine led to

279   complete loss of binding, which is consistent with it forming a hydrogen bond to a

280   side-chain asparagine but also being part of a relatively well packed region of the

281   binding site that is mostly buried upon binding. T66 is located on the edge of the

282   binding site and appears to provide hydrophobic contacts through its methyl group

283   with the methyl side-chain of an alanine of the peptide; mutation of this residue

284   resulted in a partial loss of binding. Interestingly, mutation of E64, which is location

285   in an appropriate position to form some hydrogen bonds to the peptide resulted in a

286   slight increase in binding, although charged residues on the edge of protein:protein

287   interfaces are known to contribute primarily to specificity rather than affinity [32].

288   Specifically, the cost of desolvating charged residues such as glutamate is not

289   compensated for by the hydrogen bonds that may be formed with the binding partner.

290   Y37 is located outside the direct binding site in the apo-crystal structure; the loss of

291   affinity could arise from long-range effects, such as destabilization of the position of

292   nearby loops. In general, the effects of the mutations are consistent with the model of

293   the interaction.

294

295   **The multivalency of the CSP repeat region**

296

297   The binding mode of the F_{AB} fragment to the $(NANP)_6$ peptide is centered on

298   two proline residues from two non-adjacent NANP-repeats (**Fig. 3A, C**). These cyclic

13

299   side-chains are hydrophobic in character and are buried deeply in the core of the F_{AB}

300   antigen binding site, into hydrophobic pockets formed by Y38 and Y56 of the light

301   chain and the interface between the two chains. In contrast, the polar asparagine

302   residues on the sides of the helix are involved in hydrogen bonding interactions with a

303   number of polar residues on the edge of the binding site, such as N57 of the heavy

304   chain. Due to the twisting of the $(NANP)_6$ repeat, the binding epitope of the peptide is

305   2.5-3 alternate NANP repeats, with a symmetrical epitope available for binding on the

306   opposite face (**Fig. 4A**). Thus, this binding mode is consistent with the stoichiometry

307   of the binding observed in the ITC measurements, where we observed a stoichiometry

308   of two 2A10 F_{AB} fragments per $(NANP)_6$ peptide. To investigate whether this binding

309   mode was also compatible with the indication from ITC that ~10.7 2A10 F_{AB}

310   fragments, or six antibodies (containing 12 F_{AB} domains) could bind the CSP protein

311   (**Table 1**), we extended the peptide to its full length. It is notable that the slight twist

312   in the NANP helix results in the epitope being offset along the length of the repeat

313   region, thereby allowing binding of ten 2A10 F_{AB} fragments (**Fig. 4B**). Six 2A10

314   antibodies can bind if two antibodies interact by a single F_{AB} domain and the other

315   four interact with both F_{AB} domains. The observation that the F_{AB} fragments bind

316   sufficiently close to each other to form hydrogen bonds also explains the observation

317   from the ITC that the complexes with rCSP, which allow adjacent F_{AB} fragment

318   binding, have more favorable binding enthalpy, i.e. the additional bonds formed

319   between adjacent F_{AB} fragments further stabilize the complex and lead to greater

320   affinity (**Table 1**). Thus, the initially surprising stoichiometry that we observe through

321   ITC appears to be quite feasible based on the structure of the NANP-repeat region of

322   the rCSP protein and the nature of the rCSP-2A10 complex. It is also clear that the

323   effect of antibody binding to this region would be to prevent the linker flexing

14

324 between the N- and C-terminal domains and maintaining normal physiological

325 function, explaining the neutralizing effect of the antibodies.

326

327 **Identification of endogenous (NANP)$_n$ specific B cells to determine the BCR**

328 **repertoire**

329

330 We next set out to determine the implications of our structure for the B cell

331 response to CSP. Because the CSP protein could conceivably cross-link multiple B

332 cell receptors (BCRs) we hypothesized that the B cell response might be T-

333 independent. As a tool to test this hypothesis we used (NANP)$_n$-based tetramers to

334 identify and phenotype antigen specific B cells in mice immunized with *P. berghei*

335 sporozoites expressing the repeat region of the *P. falciparum* CSP (*P. berghei* CS^{Pf})

336 [15]. The tetramers are formed by the binding of 4 biotinylated (NANP)$_9$ repeats with

337 streptavidin conjugated phycoerythrin (PE) or allophycocyanin (APC). To validate

338 our tetramer approach, mice were immunized with either *P. berghei* CS^{Pf} or another

339 line of *P. berghei* with a mutant CSP (*P. berghei* CS^{5M}) that contains the endogenous

340 (*P. berghei*) repeat region, which has a distinct repeat sequence (PPPPNPND)$_n$.

341 (NANP)$_n$-specific cells were identified with two tetramer probes bound to different

342 conjugates to exclude B cells that are specific for the PE or APC components of the

343 tetramers which are numerous in mice [33]. We found that mice immunized with *P.*

344 *berghei* CS^{Pf} sporozoites developed large tetramer double positive populations, which

345 had class switched (**Fig. 5A** and **B**). In contrast, the number of tetramer double

346 positive cells in mice receiving control parasites was the same as in unimmunized

347 mice; moreover these cells were not class switched and appeared to be naïve

348 precursors indicating that our tetramers are identifying bona-fide (NANP)$_n$-specific

15

349   cells (**Fig. 5B** and **C**). Further analysis of the different populations of B cells showed

350   that most B cells present at this time-point were $GL7^+ CD38^-$ indicating that they are

351   GC B cells in agreement with results from a recent publication [34] (**Fig. 5B** and **D**).

352   Given that T cells are required to sustain GC formation beyond ~3 days these data

353   indicate that a T-dependent response can develop to CSP following sporozoite

354   immunization [35].

355

356   **The B cell response to the $(NANP)_n$ repeat has both T-independent and T-**

357   **dependent components**

358

359   Our previous data showing GC formation among $(NANP)_n$ specific B cells

360   was indicative of a T-dependent response. To determine whether there might also be a

361   T-independent component to the B cell response we immunized $CD28^{-/-}$ mice as well

362   as C57BL/6 controls with *P. berghei* CS^{Pf} radiation attenuated sporozoites (RAS) and

363   measured serum $(NANP)_n$ specific antibody by ELISA and the B cell response using

364   our Tetramers. $CD28^{-/-}$ mice have CD4+ T cells but they are unable to provide help to

365   B cell responses [36]. Interestingly 4 days post immunization there were comparable

366   IgM and IgG anti-$(NANP)_n$ responses in the $CD28^{-/-}$ mice and control animals (**Fig.**

367   **6A**), indicative of a T-independent component to immunity. However by day 27 post

368   immunization there was no detectable IgM or IgG antibody specific for $(NANP)_n$ in

369   the $CD28^{-/-}$ mice suggesting the T-independent response is short-lived. We further

370   analyzed $(NANP)_n$ specific B cell responses using our tetramers, in particular

371   examining the number and phenotype (plasmablast vs GC B cell) of activated IgD^-

372    $Tetramer^+$ cells (**Fig. 6B**). In agreement with our antibody data, similar numbers of

373   antigen specific B cells were seen at 4 days post immunization in the $CD28^{-/-}$ and

374   control mice and most of these cells were plasmablasts (**Fig. 6C**). However by 7 days

375   post immunization the number of antigen specific cells declines in the $CD28^{-/-}$ mice as

376   the T dependent GC reaction begins to predominate. Thus CSP on the surface of

377   sporozoites is able to induce short-lived T-independent B cell response, but

378   subsequently T-dependent responses predominate.

379

380   We wanted to know if to induce a T-independent response it was necessary for

381   CSP to be presented on the surface of the sporozoite or if free rCSP was sufficient.

382   We found that indeed rCSP could induce a T-independent response as evidenced by

383   similar IgM and IgG levels and $IgD^-Tetramer^+$ responses 4 days post immunization in

384   control and $CD28^{-/-}$ mice (**Fig. 6D, E**). Finally we were concerned that there may be

385   some residual $CD4^+$ T cell help in the $CD28^{-/-}$ mice so we performed experiments in

386   which we used the antibody GK1.5 to deplete $CD4^+$ T cells [37]. In agreement with

387   our previous data we found that sporozoites (live or RAS) and rCSP induced IgM

388   responses in CD4 depleted mice, though we were unable to detect a significant IgG

389   response (**Fig. S4 A**). We also detected primed antigen specific B cells in GK1.5

390   treated mice following RAS or rCSP immunized mice 4 days post-immunization,

391   albeit at lower levels than in mice treated with isotype control antibodies (**Fig. S4 B**).

392   Overall our data with GK1.5 depleted mice support our results in the $CD28^{-/-}$ model.

393

394   **A restricted repertoire of BCRs can bind to the $(NANP)_n$ repeat**

395

396   Our ability to identify and sort $(NANP)_n$ specific B cells with our tetramers

397   also allows us to examine the repertoire of antibodies that can bind the $(NANP)_n$ by

398   sequencing the BCRs of the identified cells. While the repeat structure of CSP has

399   been hypothesized to induce a broad polyclonal response [38], an alternative

400   hypothesis is that the antigenically simple structure of the repeat epitope might only

401   be recognized by a small number of naïve B cells. We therefore sorted $(NANP)_n$-

402   specific cells 35 days post immunization of BALB/C mice with sporozoites. We

403   performed this analysis in BALB/C mice as this is the background of mice from

404   which the 2A10 antibody was derived. We then prepared cDNA from the cells and

405   amplified the heavy and kappa chain sequences using degenerate primers as described

406   previously [39,40]. Heavy and light chain libraries were prepared from 4 immunized

407   mice as well as from 3 naïve mice from which we bulk sorted B cells as controls. We

408   obtained usable sequences from 3 of the 4 mice for both the heavy chain and kappa

409   chain. Analysis of the heavy chain revealed that in each mouse 3 or 4 V regions

410   dominated the immune response (**Fig. 7A**). The V regions identified (IGHV1-20;

411   IGHV1-26; IGHV1-34 and IGHV5-9) were generally shared among the mice. As a

412   formal measure of the diversity of our V region usage in the $(NANP)_n$ specific cells

413   and the bulk B cells from naïve mice we calculated the Shannon entropy for these

414   populations. This analysis formally demonstrated that the diversity of the antigen

415   specific B cells was significantly lower than the diversity of the repertoire in naïve

416   mice (**Fig. 7B**). We further found that each V region was typically associated with the

417   same D and J sequences even in different mice. For example, IGHV1-20 was

418   typically associated with J4, IGHV5-9 with J4 while in different mice IGHV1-34 was

419   variously paired with J1 or J4 (**Fig. 7C**). Similar results were obtained for the kappa

420   chain with the response dominated by IGKV1-135; IGKV5-43/45; IGKV1-110;

421   IGKV1-117 and IGKV14-111 (**Fig. 7D and E**). The V regions were typically paired

422   with the same J regions even in different mice (**Fig. 7F**), for example IGKV5.43/45

423   was typically paired with IGKJ5 or IGKJ2 and IGKV1-110 was typically paired with

424   IGKJ5, although IGKV1-135 was typically more promiscuous. One limitation of our

425   high throughput sequencing approach is that the degenerate primers only amplified

426   ~70% of the known IGHV and IGKV sequences in naïve mice, suggesting that we

427   may not capture the full diversity of the response. However, comparison with the 5

428   published antibody sequences (**S2** and **S3 Table**) that include IGHV-1-20, IGKV5-45

429   and IGKV1-110 reveals that we are likely capturing the bulk of the antibody diversity.

430   Together these data suggest that the number of B cell clones responding to CSP may

431   be limited, potentially reducing the ability of the immune system to generate effective

432   neutralizing antibodies.

433

434   **CSP-binding antibodies undergo somatic hypermutation to improve affinity**

435

436   Finally we were interested in knowing if the GC reaction we could see

437   following sporozoite immunization was inducing higher affinity antibodies. We

438   therefore examined our deep sequencing data to determine if CSP-specific antibodies

439   had undergone somatic hypermutation (SHM) that would be indicative of B cells

440   specific for CSP entering the GC. Taking advantage of the fact that our kappa chain

441   primers capture the entire V-J sequences of the antibodies we sequenced we asked: 1)

442   if the kappa chains shared between immune animals differed from the germline

443   (providing evidence of SHM) and 2) if the mutations were conserved between

444   different mice indicative of directed selection. Analysis of the reads from the kappa

445   chains of the three immune mice showed that these had a much higher degree of

446   mutation than bulk B cells from naïve mice, demonstrating SHM in the CSP-specific

447   antibodies (**Fig. 8A**). We further examined each specific common kappa chain in turn

448   (IGVK1-110; IGKV1-135; IGVK5-43/45) comparing the sequences obtained from

19

449   naïve B cells and $(NANP)_n$ specific cells in immune mice. This analysis showed that

450   while, as expected, sequences from naïve mice contained few mutations, the

451   sequences from immune mice had much higher levels of SHM. Importantly mutations

452   were found to be concentrated in the CDR loops, and were frequently shared by

453   immunized mice providing strong circumstantial evidence for affinity maturation

454   (**Fig. 8B**; data for IGVK1-110 only shown).

455

456   To directly test if CSP-binding antibodies undergo affinity maturation we

457   expressed the predicted germline precursor to the 2A10 antibody (2A10 gAb) in

458   HEK293T cells. We identified the predicted germline precursors of the 2A10 heavy

459   and light chains using the program V-quest [41] (**Figs. S5** and **S6**). This analysis

460   identified the heavy chain as IGHV9-3; IGHD1-3; IGHJ4 and the light chain as

461   IGKV10-94;IGKJ2, with the monoclonal antibody carrying 6 mutations in the heavy

462   chain and 7 in the light chain. The 2A10 gAb had considerably lower binding in

463   ELISA assays compared to the 2A10 mAb itself (**Fig. 8C**), indicative that affinity

464   maturation had taken place in this antibody. To determine the relative contribution of

465   mutations in the heavy and light chain to enhancing binding we also made hybrid

466   antibodies consisting of the mAb heavy chain and the gAb light chain and vice versa.

467   Interestingly mutations in the light chain were almost entirely sufficient to explain the

468   enhanced binding by the mAb compared to the gAb (**Fig. 8C**).

469

470   To identify the specific mutations that were important we introduced the

471   mutations individually into the gAb light chain construct. We prioritized mutations

472   that were shared with the 27E antibody which has previously been found to be

473   clonally related to 2A10 having been isolated from the same mouse and which shares

20

474   the same germline heavy and light chains as the 2A10 mAb [20]. We found that two

475   mutations (L114F and T117V) in the CDR3 of the light chain appeared to account for

476   most of the gain in binding (**Fig. 8C**). The effect of these antibodies appeared to be

477   additive rather than synergistic as revealed by experiments in which we introduced

478   these mutations simultaneously (**Fig. 8D**). A further mutation close to the light chain

479   CDR2 (H68Y) also caused a modest increase in binding. As expected mutations in the

480   heavy chains appeared generally less important for increasing binding though M39I,

481   N59I and T67F all gave modest increases in binding (**Fig. 8E**). Collectively our data

482   suggest that CSP repeat antibodies can undergo SHM in GCs resulting in affinity

483   maturation, however the antibody response may be limited by the number of naïve B

484   cells that can recognize and respond to this antigen.

485

Discussion

486

487

488   Here we provide an analysis of the structure of a *Plasmodium falciparum*

489   sporozoite-neutralizing antibody (2A10). Having obtained this structure we further

490   modeled the binding 2A10 with its antigen target, the repeat region of CSP, and

491   provide a thermodynamic characterization of this interaction. Finally, we used novel

492   tetramer probes to identify and sort antigen specific B cells responding to sporozoite

493   immunization in order to measure the diversity and maturation of the antibody

494   response. We found that the avidity of 2A10 for the rCSP molecule was in the

495   nanomolar range, which was much higher than the affinity previously predicted from

496   competition ELISAs with small peptides [22,23]. This affinity is a consequence of the

497   multivalent nature of the interaction, with up to 6 antibodies being able to bind to each

498   rCSP molecule. Our model suggests that to spatially accommodate this binding the

499   antibodies must surround CSP in an off-set manner, which is possible due to the slight

500   twist in the helical structure that CSP can adopt. It is notable that the twisted,

501   repeating arrangement of the CSP linker is the only structure that would allow binding

502   in the stoichiometry observed through the ITC. We further found that the diversity of

503   the antibody repertoire to the CSP repeat was limited, perhaps due to the relative

504   simplicity of the target epitope. However, these antibodies have undergone affinity

505   maturation to improve affinity, potentially allowing protective immune responses to

506   develop.

507

508   Using ITC we determined the dissociation constant of 2A10 for rCSP to be 2.7

509   nM, which is not unusual for a mouse mAb. However it is a tighter interaction than

510   that predicted from competition ELISAs, which predicted a micro-molar affinity

22

511   [22,23]. However, these competition ELISAs were performed with short peptides

512   rather than rCSP. Indeed, when we performed ITC with a short peptide and F_{AB}

513   fragments we too obtained a dissociation constant in the micro-molar range (0.42

514   μM). The difference between the F_{AB} binding to the peptide and the tight interaction

515   of the antibody binding to full length CSP appears to be driven by a high avidity,

516   multivalent interaction. There is also additional enthalpic stabilization (per F_{AB}

517   domain) in the 2A10:CSP complex, although this is partially offset by the increased

518   entropic cost associated with combining a large number of separate molecules into a

519   single complex. One caveat of these data is that we used a slightly truncated repeat in

520   our recombinant CSP, however it is likely that longer repeats will have further

521   stabilization of the interaction that could result in even higher affinity interaction

522   between CSP and binding antibodies.

523

524   The mechanism of sporozoite neutralization remains unclear, however our

525   structural data may provide some insights. Repeat specific antibodies can directly

526   neutralize sporozoites (without complement or other cell mediators) in the

527   circumsporozoite reaction [8,42]. Morevoer F_{AB} fragments alone are sufficient to

528   block invasion [42,43]. However, it is well established that activation for complement

529   and cell mediated immunity is important for the action of blood stage-specific

530   antibodies [44,45]. It has also been suggested that the CSP repeat might act as a hinge

531   allowing the N-terminal domain to mask the C-terminal domain which is believed to

532   be important for binding to and invading hepatocytes [10]. Cleavage of this N-

533   terminal domain is therefore required to expose the C-terminal domain and facilitate

534   invasion [10]. Antibody binding as observed here may disrupt this process in several

535   ways, either by opening the hinge to induce the premature exposure of the C-terminal

23

536   domain. Alternatively since the repeat region is directly adjacent to the proteolytic

537   cleavage site, anti-repeat antibodies might function by sterically hindering access of

538   the protease to CSP, thus preventing sporozoite invasion of the hepatocyte. One

539   possible consequence of the requirement for mutivalency to increase the avidity of the

540   antibody, is that antibodies with different binding modes may interfere with each

541   other limiting their effectiveness.

542

543   Our results uncovering how neutralizing antibodies bind to CSP has several

544   implications for understanding the development of the immune response to CSP.

545   Notably the finding that the CSP molecule can be bound by multiple antibodies/B cell

546   receptors raises the possibility that this molecule can indeed crosslink multiple BCRs

547   and potentially act as a type-II T independent antigen [17]. We find that indeed there

548   is a T-independent component to the response to CSP, though T cells are required to

549   sustain the immune response beyond day 7. As such the response to CSP appears

550   follow a similar process to that seen for several oligomeric viral entry proteins, which

551   induce a mix of T-independent and T-dependent responses [18,19]. It maybe that T-

552   independent responses are driven by the density of CSP molecules on the sporozoite

553   surface; however, rCSP can also induce a small T-independent response. This

554   suggests that the CSP protein alone is sufficient to crosslink multiple BCRs on the B

555   cell surface which is consistent with our structural model. Interestingly, the

556   RTS,S/AS01 vaccine based on that contains 18 CSP repeats and does appear to induce

557   high titers of anti-CSP antibodies which initially decline rapidly and are then more

558   stable [4,46]. This may be consistent with the induction of a short-lived a type-II T-

559   independent plasmablast response (accounting for the initial burst of antibodies),

560   followed by a T-dependent response (which may be the basis of the more sustained

24

561   antibody titers). The relative contributions of short-lived antibody production and

562   long-term B cell memory to protection is an area for future investigation.

563

564   The finding of a limited repertoire in the BCR sequences specific for the

565     $(NANP)_n$ repeat contradicts previous suggestions that the response to CSP might be

566   broad and polyclonal [38]. One explanation for this limited antibody diversity is that

567   the antigenic simplicity of the CSP repeat region limits the range of antibodies that are

568   capable of responding. A prior example of this is the antibodies to the Rhesus (Rh) D

569   antigen. The RhD antigen differs from RhC by only 35-36 amino acids, resulting in

570   the creation of a minimal B cell epitope [47]. The repertoire of antibodies that can

571   bind this epitope are accordingly limited and mainly based on the VH3-33 gene

572   family [48]. Another potential explanation for a limited antibody repertoire could be

573   that the $(NANP)_n$ repeat shares structural similarity with a self-antigen as is

574   speculated to happen with meningococcus type B antigens [49], however it is not

575   clear what this self-antigen might be. One potential outcome of this finding is that if

576   each B cell clone has a finite burst size this may limit the magnitude of the overall B

577   cell response.

578

579   One area for future investigation is to determine the binding modes and

580   sporozoite neutralizing capacities of other antibodies in the response. It is clear that

581   not all CSP-repeat binding antibodies have the same capacity for sporozoite

582   neutralization [7]. As such the finding of a limited repertoire of responding B cells

583   may lead to the possibility that some people have holes in their antibody repertoires

584   limiting their ability to make neutralizing antibodies. This may explain why, while

25

585   there is a broad correlation between ELISA tires of antibodies to the CSP repeat and

586   protection following RTS,S vaccination, there is no clear threshold for protection [4].

587

588   While our work has been performed with mouse antibodies, there are major

589   similarities between mouse and human antibody loop structure [50]. The main

590   difference between the two species is the considerably more diverse heavy chain

591   CDR3 regions that are found in human antibodies [51]. Consequently, this leads to a

592   much larger number of unique clones found in humans compared to mice. However,

593   the number of different V, D and J genes and the recombination that follows are

594   relatively similar between humans and mice [52]. From our data it can be observed

595   that while the BCR repertoire was restricted in the V gene usage, these different V

596   gene populations were represented in multiple unique clones, suggesting that

597   increasing the number of clones is unlikely to substantially increase V-region usage.

598   Our analysis was also performed on inbred mice which may also limit repertoire

599   diversity, however studies on the human IGHV locus reveal that in any given

600   individual ~80% V region genes are identical between the maternal and paternal allele

601   i.e. heterozygosity is not a major driver of human V region diversity [53,54]. It is

602   notable that all 4 human monoclonal antibodies described to date from different

603   volunteers share the use of the IGHV3-30 gene family [21,22], suggesting that in

604   humans as well as mice there may indeed be a constrained repertoire of responding B

605   cells.

606

607   Overall our data provide important insights into how the antibody response to

608   CSP develops. Our results also help explain why relatively large amounts of

609   antibodies are required for sporozoite neutralization and suggest that the ability to

610   generate an effective B cell response may be limited by the very simplicity of the

611   repeat epitope. These data support previous suggestions that CSP may be a

612   suboptimal target for vaccination. However, we also find that CSP binding antibodies

613   can undergo somatic hypermutation and reach high affinities. This suggests if we can

614   develop vaccination strategies to diversify the repertoire of responding B cells and

615   favor the GC response it may be possible to generate long-term protective immunity

616   targeting this major vaccine candidate antigen.

617

618

27

619 **Methods**

620

621 **Ethics statement**

622 All animal procedures were approved by the Animal Experimentation Ethics

623 Committee of the Australian National University (Protocol numbers: A2013/12;

624 A2014/62 and A2015/76). All research involving animals was conducted in

625 accordance with the National Health and Medical Research Council's (NHMRC)

626 Australian Code for the Care and Use of Animals for Scientific Purposes and the

627 Australian Capital Territory Animal Welfare Act 1992.

628

629 **Mice, Immunizations and Cell Depletions**

630 BALB/C, C57BL/6 or CD28$^{-/-}$ [55] mice (bred in-house at the Australian National

631 University) were immunized IV with 5 x 10^4 *P. berghei* CS^{5M} sporozoites expressing

632 mCherry [56] or 5 x 10^4 *P. berghei* CS^{Pf} sporozoites dissected by hand from the

633 salivary glands of *Anopheles stephensi* mosquitoes. Mice were either infected with

634 live sporozoites and then treated with 0.6mg choloroquine IP daily for 10 days or

635 immunized with irradiated sporozoites (15kRad). For immunization with rCSP, 30ug

636 rCSP was emulsified in Imject™ Alum according to the manufacturer's instructions

637 (ThermoFisher Scientific) and delivered intra-peritoneally. To deplete CD4+ T cells

638 mice were treated with two doses of 100ug GK1.5 antibody on the 2 days prior to

639 immunization (BioXCell); control mice received an irrelevant isotype control

640 antibody (LTF2; BioXCell).

641

28

Flow Cytometry and sorting

Single cell preparations of lymphocytes were isolated from the spleen of immunized mice and were stained for flow cytometry or sorting by standard procedures. Cells were stained with lineage markers (anti-CD3, clone 17A2; anti-GR1, clone RB6-8C5 and anti-NKp46, clone 29A1.4) antibodies to B220 (clone RA3-6B2), IgM (clone II/41), IgD (clone 11-26c2a), GL7 (clone GL7), CD38 (clone 90), CD138 (clone 281-2) and (NANP)$_9$ tetramers conjugated to PE or APC. Antibodies were purchased from Biolegend while tetramers were prepared in house by mixing biotinylated (NANP)$_9$ peptide with streptavidin conjugated PE or APC (Invitrogen) in a 4:1 molar ratio. Flow-cytometric data was collected on a BD Fortessa flow cytometer (Becton Dickinson) and analyzed using FlowJo software (FlowJo). Where necessary cells were sorted on a BD FACs Aria I or II machine.

Sequencing of (NANP)$_n$ specific cells and BCR analysis

Single cell suspensions from the spleens of immunized mice were stained with (NANP)$_n$ tetramers and antibodies to B cell markers as described in the supplementary experimental procedures. Antigen specific cells were sorted on a FACS ARIA I or II instrument prior to RNA extraction with the Arturus Picopure RNA isolation kit (Invitrogen) and cDNA preparation using the iScript cDNA synthesis kit (BioRad). BCR sequences were amplified using previously described heavy and kappa chain primers including adaptor sequences allowing subsequent indexing using the Nextera indexing kit (Illumina). Analysis was performed in house using R-scripts and the program MiXCR as described in supplementary experimental procedures.

667 **Binding of antibody variants**

668 Variants of the 2A10 antibody were expressed in HEK293 T cells (a kind gift of

669 Carola Vinuesa, Australian National University) as described in the supplemental

670 experimental procedures. Binding to the CSP repeat was tested by ELISA and ITC

671 using standard techniques as described in the supplementary experimental procedures.

672

673 **Statistical Analysis**

674 Statistical analysis was performed using Prism6 (GraphPad) for simple T tests and

675 one-way ANOVAs from single experiments. Where data were pooled from multiple

676 experiments, analysis was performed using linear mixed models in R version 3.3.3 (R

677 foundation for Statistical Computing). Linear mixed models are a regression analysis

678 model containing both fixed and random effects: fixed effects being the

679 variable/treatment under examination, whilst random effects are unintended factors

680 that may influence the variable being measured. If significance was found from

681 running a linear mixed model, pair-wise comparisons of the least significant

682 differences of means (LSD) was undertaken to determine at which level interactions

683 were occurring. Statistical significance was assumed if the p-value was < 0.05 for a

684 tested difference. (ns = not significant, *= $p < 0.5$, ** = $p < 0.01$, *** = $p < 0.001$,

685 **** = $p < 0.0001$).

686

687

688 **Data Deposition**

689 Sequence data generated in this paper is deposited at the NCBI BioProject database

690 accession number PRJNA352758. Atomic coordinates and related experimental data

30

691   for structural analyses are deposited in the Protein Data Bank (PDB) with PDB codes

692   5ZSF and 5T0Y.

31

693 **Acknowledgments**

694

700

References

1. World Health Organization (2016) World Malaria Report 2016. Geneva: World Health Organization.

2. Casares S, Brumeanu TD, Richie TL (2010) The RTS,S malaria vaccine. Vaccine 28: 4880-4894.

3. RTS,S Clinical Trials Partnership (2015) Efficacy and safety of RTS,S/AS01 malaria vaccine with or without a booster dose in infants and children in Africa: final results of a phase 3, individually randomised, controlled trial. Lancet 386: 31-45.

4. White MT, Bejon P, Olotu A, Griffin JT, Riley EM, et al. (2013) The relationship between RTS,S vaccine-induced antibodies, CD4(+) T cell responses and protection against Plasmodium falciparum infection. PLoS One 8: e61395.

5. Nussenzweig RS, Vanderberg J, Most H, Orton C (1967) Protective immunity produced by the injection of x-irradiated sporozoites of plasmodium berghei. Nature 216: 160-162.

6. Seder RA, Chang LJ, Enama ME, Zephir KL, Sarwar UN, et al. (2013) Protection against malaria by intravenous immunization with a nonreplicating sporozoite vaccine. Science 341: 1359-1365.

7. Hollingdale MR, Nardin EH, Tharavanij S, Schwartz AL, Nussenzweig RS (1984) Inhibition of entry of Plasmodium falciparum and P. vivax sporozoites into cultured cells; an in vitro assay of protective antibodies. J Immunol 132: 909-913.

8. Yoshida N, Nussenzweig RS, Potocnjak P, Nussenzweig V, Aikawa M (1980) Hybridoma produces protective antibodies directed against the sporozoite stage of malaria parasite. Science 207: 71-73.

9. Dame JB, Williams JL, McCutchan TF, Weber JL, Wirtz RA, et al. (1984) Structure of the gene encoding the immunodominant surface antigen on the sporozoite of the human malaria parasite Plasmodium falciparum. Science 225: 593-599.

10. Coppi A, Natarajan R, Pradel G, Bennett BL, James ER, et al. (2011) The malaria circumsporozoite protein has two functional domains, each with distinct roles as sporozoites journey from mosquito to mammalian host. J Exp Med 208: 341-356.

11. Zavala F, Cochrane AH, Nardin EH, Nussenzweig RS, Nussenzweig V (1983) Circumsporozoite proteins of malaria parasites contain a single immunodominant region with two or more identical epitopes. J Exp Med 157: 1947-1957.

12. Gardner MJ, Hall N, Fung E, White O, Berriman M, et al. (2002) Genome sequence of the human malaria parasite Plasmodium falciparum. Nature 419: 498-511.

13. Zeeshan M, Alam MT, Vinayak S, Bora H, Tyagi RK, et al. (2012) Genetic variation in the Plasmodium falciparum circumsporozoite protein in India and its relevance to RTS,S malaria vaccine. PLoS One 7: e43430.

14. Espinosa DA, Gutierrez GM, Rojas-Lopez M, Noe AR, Shi L, et al. (2015) Proteolytic Cleavage of the Plasmodium falciparum Circumsporozoite Protein Is a Target of Protective Antibodies. J Infect Dis 212: 1111-1119.

15. Persson C, Oliveira GA, Sultan AA, Bhanot P, Nussenzweig V, et al. (2002) Cutting edge: a new tool to evaluate human pre-erythrocytic malaria vaccines:

749   rodent parasites bearing a hybrid Plasmodium falciparum circumsporozoite
750   protein. J Immunol 169: 6681-6685.
751 16. Schofield L, Uadia P (1990) Lack of Ir-Gene Control in the Immune-Response to
752   Malaria .1. A Thymus-Independent Antibody-Response to the Repetitive
753   Surface Protein of Sporozoites. Journal of Immunology 144: 2781-2788.
754 17. Defrance T, Taillardet M, Genestier L (2011) T cell-independent B cell memory.
755   Current Opinion in Immunology 23: 330-336.
756 18. Bachmann MF, Hengartner H, Zinkernagel RM (1995) T helper cell-independent
757   neutralizing B cell response against vesicular stomatitis virus: role of antigen
758   patterns in B cell induction? Eur J Immunol 25: 3445-3451.
759 19. Schodel F, Peterson D, Zheng J, Jones JE, Hughes JL, et al. (1993) Structure of
760   hepatitis B virus core and e-antigen. A single precore amino acid prevents
761   nucleocapsid assembly. J Biol Chem 268: 1332-1337.
762 20. Anker R, Zavala F, Pollok BA (1990) VH and VL region structure of antibodies
763   that recognize the (NANP)3 dodecapeptide sequence in the circumsporozoite
764   protein of Plasmodium falciparum. Eur J Immunol 20: 2757-2761.
765 21. Foquet L, Hermsen CC, van Gemert GJ, Van Braeckel E, Weening KE, et al.
766   (2014) Vaccine-induced monoclonal antibodies targeting circumsporozoite
767   protein prevent Plasmodium falciparum infection. J Clin Invest 124: 140-144.
768 22. Chappel JA, Rogers WO, Hoffman SL, Kang AS (2004) Molecular dissection of
769   the human antibody response to the structural repeat epitope of Plasmodium
770   falciparum sporozoite from a protected donor. Malar J 3: 28.
771 23. Zavala F, Tam JP, Hollingdale MR, Cochrane AH, Quakyi I, et al. (1985)
772   Rationale for development of a synthetic vaccine against Plasmodium
773   falciparum malaria. Science 228: 1436-1440.
774 24. Cerami C, Frevert U, Sinnis P, Takacs B, Clavijo P, et al. (1992) The basolateral
775   domain of the hepatocyte plasma membrane bears receptors for the
776   circumsporozoite protein of Plasmodium falciparum sporozoites. Cell 70:
777   1021-1033.
778 25. Braden BC, Poljak RJ (1995) Structural features of the reactions between
779   antibodies and protein antigens. FASEB J 9: 9-16.
780 26. Plassmeyer ML, Reiter K, Shimp RL, Jr., Kotova S, Smith PD, et al. (2009)
781   Structure of the Plasmodium falciparum circumsporozoite protein, a leading
782   malaria vaccine candidate. J Biol Chem 284: 26951-26963.
783 27. Kelly SM, Jess TJ, Price NC (2005) How to study proteins by circular dichroism.
784   Biochim Biophys Acta 1751: 119-139.
785 28. Shen Y, Maupetit J, Derreumaux P, Tuffery P (2014) Improved PEP-FOLD
786   Approach for Peptide and Miniprotein Structure Prediction. J Chem Theory
787   Comput 10: 4745-4758.
788 29. Ghasparian A, Moehle K, Linden A, Robinson JA (2006) Crystal structure of an
789   NPNA-repeat motif from the circumsporozoite protein of the malaria parasite
790   Plasmodium falciparum. Chem Commun (Camb): 174-176.
791 30. Sela-Culang I, Alon S, Ofran Y (2012) A systematic comparison of free and
792   bound antibodies reveals binding-related conformational changes. J Immunol
793   189: 4890-4899.
794 31. Sircar A, Gray JJ (2010) SnugDock: paratope structural optimization during
795   antibody-antigen docking compensates for errors in antibody homology
796   models. PLoS Comput Biol 6: e1000644.

797 32. Davis SJ, Davies EA, Tucknott MG, Jones EY, van der Merwe PA (1998) The
798   role of charged residues mediating low affinity protein-protein recognition at
799   the cell surface by CD2. Proc Natl Acad Sci U S A 95: 5490-5494.
800 33. Pape KA, Taylor JJ, Maul RW, Gearhart PJ, Jenkins MK (2011) Different B cell
801   populations mediate early and late memory during an endogenous immune
802   response. Science 331: 1203-1207.
803 34. Keitany GJ, Kim KS, Krishnamurty AT, Hondowicz BD, Hahn WO, et al. (2016)
804   Blood Stage Malaria Disrupts Humoral Immunity to the Pre-erythrocytic
805   Stage Circumsporozoite Protein. Cell Rep 17: 3193-3205.
806 35. de Vinuesa CG, Cook MC, Ball J, Drew M, Sunners Y, et al. (2000) Germinal
807   centers without T cells. J Exp Med 191: 485-494.
808 36. Ferguson SE, Han S, Kelsoe G, Thompson CB (1996) CD28 is required for
809   germinal center formation. J Immunol 156: 4576-4581.
810 37. Goronzy J, Weyand CM, Fathman CG (1986) Long-term humoral
811   unresponsiveness in vivo, induced by treatment with monoclonal antibody
812   against L3T4. J Exp Med 164: 911-925.
813 38. Schofield L (1990) The circumsporozoite protein of Plasmodium: a mechanism of
814   immune evasion by the malaria parasite? Bull World Health Organ 68 Suppl:
815   66-73.
816 39. Arnaout R, Lee W, Cahill P, Honan T, Sparrow T, et al. (2011) High-resolution
817   description of antibody heavy-chain repertoires in humans. PLoS One 6:
818   e22365.
819 40. Busse CE, Czogiel I, Braun P, Arndt PF, Wardemann H (2014) Single-cell based
820   high-throughput sequencing of full-length immunoglobulin heavy and light
821   chain genes. Eur J Immunol 44: 597-603.
822 41. Brochet X, Lefranc MP, Giudicelli V (2008) IMGT/V-QUEST: the highly
823   customized and integrated system for IG and TR standardized V-J and V-D-J
824   sequence analysis. Nucleic Acids Res 36: W503-508.
825 42. Potocnjak P, Yoshida N, Nussenzweig RS, Nussenzweig V (1980) Monovalent
826   fragments (Fab) of monoclonal antibodies to a sporozoite surface antigen
827   (Pb44) protect mice against malarial infection. J Exp Med 151: 1504-1513.
828 43. Stewart MJ, Nawrot RJ, Schulman S, Vanderberg JP (1986) Plasmodium berghei
829   sporozoite invasion is blocked in vitro by sporozoite-immobilizing antibodies.
830   Infect Immun 51: 859-864.
831 44. Bouharoun-Tayoun H, Attanath P, Sabchareon A, Chongsuphajaisiddhi T, Druilhe
832   P (1990) Antibodies that protect humans against Plasmodium falciparum
833   blood stages do not on their own inhibit parasite growth and invasion in vitro,
834   but act in cooperation with monocytes. J Exp Med 172: 1633-1641.
835 45. Boyle MJ, Reiling L, Feng G, Langer C, Osier FH, et al. (2015) Human antibodies
836   fix complement to inhibit Plasmodium falciparum invasion of erythrocytes
837   and are associated with protection against malaria. Immunity 42: 580-590.
838 46. White MT, Bejon P, Olotu A, Griffin JT, Bojang K, et al. (2014) A combined
839   analysis of immunogenicity, antibody kinetics and vaccine efficacy from
840   phase 2 trials of the RTS,S malaria vaccine. BMC Med 12: 117.
841 47. Avent ND, Madgett TE, Lee ZE, Head DJ, Maddocks DG, et al. (2006) Molecular
842   biology of Rh proteins and relevance to molecular medicine. Expert Rev Mol
843   Med 8: 1-20.
844 48. Chang TY, Siegel DL (1998) Genetic and immunological properties of phage-
845   displayed human anti-Rh(D) antibodies: implications for Rh(D) epitope
846   topology. Blood 91: 3066-3078.

847   49. Finne J, Leinonen M, Makela PH (1983) Antigenic similarities between brain
848   components and bacteria causing meningitis. Implications for vaccine
849   development and pathogenesis. Lancet 2: 355-357.
850   50. North B, Lehmann A, Dunbrack RL (2011) A New Clustering of Antibody CDR
851   Loop Conformations. Journal of Molecular Biology 406: 228-256.
852   51. Stanfield RL, Wilson IA (2014) Antibody Structure. Microbiology spectrum 2.
853   52. Lefranc MP, Giudicelli V, Duroux P, Jabado-Michaloud J, Folch G, et al. (2015)
854   IMGT(R), the international ImMunoGeneTics information system(R) 25 years
855   on. Nucleic Acids Res 43: D413-422.
856   53. Boyd SD, Gaeta BA, Jackson KJ, Fire AZ, Marshall EL, et al. (2010) Individual
857   variation in the germline Ig gene repertoire inferred from variable region gene
858   rearrangements. J Immunol 184: 6986-6992.
859   54. Kidd MJ, Chen Z, Wang Y, Jackson KJ, Zhang L, et al. (2012) The inference of
860   phased haplotypes for the immunoglobulin H chain V region gene loci by
861   analysis of VDJ gene rearrangements. J Immunol 188: 1333-1340.
862   55. Shahinian A, Pfeffer K, Lee KP, Kundig TM, Kishihara K, et al. (1993)
863   Differential T cell costimulatory requirements in CD28-deficient mice.
864   Science 261: 609-612.
865   56. Cockburn IA, Tse SW, Zavala F (2014) CD8+ T cells eliminate liver stage
866   Plasmodium parasites without detectable bystander effect. Infect Immun.
867   57. Bulheller BM, Hirst JD (2009) DichroCalc--circular and linear dichroism online.
868   Bioinformatics 25: 539-540.
869
870

871   **Supporting Information Legends**

872

873   **Supplementary Methods and Tables:** Contains extended methods; S1 Table (Data

874   collection and refinement statistics for the crystal structures of 2A10 F_{AB} presented in

875   this work); S2 Table (Heavy chain CDR sequences of CSP binding antibodies); S3

876   Table (Light chain CDR sequences of CSP binding immunoglobulins) and

877   supplementary references.

878

879   **S1 Fig: Theoretical (A) and experimental (B) CD spectra of the (NANP)$_6$ peptide.**

880   The computational prediction of the spectra (A) was performed using DichroCalc

881   [57], the experimental spectra was measured at 222 nm at 25 °C. A peak at 185 nm,

882   minimum at 205 nm and shoulder between 215 and 240 nm are consistent with an

883   intrinsically disordered, but not random coil, structure.

884

885   **S2 Fig: Cluster analysis for MD simulations of (NANP)$_6$ peptide.** Conformations

886   were clustered by concatenating the trajectory and performing a Jarvis-Patrick

887   analysis. The clusters are sorted by their RMSD from the first cluster (starting

888   geometry). As shown, Run 2 is stable in the starting geometry for several ns, while

889   Run 3 diverged, then reconverged to the starting geometry, where it was stable for

890   several ns. These data suggest the quasi-helical structure observed from the ab initio

891   calculations is stable, and can be spontaneously sampled, on a timescale of several ns.

892

893   **S3 Fig: Cluster analysis for MD simulations of (NANP)$_6$ peptide.** Molecular

894   dynamics simulation of the (NANP)$_6$:F_{AB} complex. Root mean square deviation

895   (RMSD) of the (NANP)$_6$:F_{AB} complex as a function of time. Independent simulations

896   are shown in green, black and red.

897

898   **S4 Fig: The B cell response to CSP has a T-independent component.** Mice either

899   treated with an anti-CD4 depleting antibody or an isotype control were immunizaed

900   with either *P. berghei* CS^{Pf} RAS, live *P. berghei* CS^{Pf} under CQ cover or rCSP. (A) 4

901   days later the IgM and IgG response to the $(NANP)_n$ repeat was analyzed by ELISA

902   (B) At the same time the number of IgD^- $Tetramer^+$ B cells was quantified in the

903   spleen. Data are from a single experiment, analyzed using linear models with

904   immunization/treatment as the experimental factor.

905

906   **S5 Fig: Alignment of 2A10 heavy chain and the predicted germline sequence**

907   Residues that are mutated away from the predicted germline sequence in more one or

908   more other antibody heavy chain (2E7 or 3D6) are highlighted in red, mutations that

909   are predicted to be involved in binding to CSP are highlighted in blue.

910

911   **S6 Fig: Alignment of 2A10 heavy chain and the predicted germline sequence**

912   Residues that are mutated away from the predicted germline sequence in both 2A10

913   and the related 2E7 antibody are highlighted in red, mutations that are predicted to be

914   involved in binding to CSP are highlighted in blue.

915

916   **Movie S1: Molecular Dynamics simulation of the solution structure of the**

917   **$(NANP)_6$ peptide**

918   Excerpt from $(NANP)_6$ run 3. The trajectory was fitted to minimize alpha-carbon

919   RMSD and then passed through a low-pass filter with a filter length of 8 frames to

920   reduce temporal aliasing.

921

922   **Movie S2: Molecular Dynamics simulation of the interaction of the $(NANP)_n$**

923   **repeat with the 2A10 F_{AB}**

924   Excerpt from $2A10:(NANP)_6$ run 3. The trajectory was fitted to minimize alpha-

925   carbon RMSD and then passed through a low-pass filter with a filter length 8 frames

926   to reduce temporal aliasing.

927   **Figure Legends**

928

929   **Fig. 1. ITC data for interactions between 2A10 F_{AB} and antigens.** (A) Titration of

930   2A10 F_{AB} with $(NANP)_6$. (B) Titration of 2A10 F_{AB} with rCSP. (C) Titration of 2A10

931   (complete antibody) with rCSP. The upper panels represent baseline-corrected power

932   traces. By convention, negative power corresponds to exothermic binding. The lower

933   panels represent the integrated heat data fitted to the independent binding sites model.

934

935   **Fig 2. Structures of the $(NANP)_6$ peptide (A), the 2A10 F_{AB} fragment (B) and the**

936   **model of the F_{AB} fragment-$(NANP)_6$ complex (C).** (A) The calculated structure of

937   the $(NANP)_6$ peptide is a helical structure containing the same hydrogen bonds

938   between a carbonyl following the proline and the amide nitrogen of the alanine, and

939   the carbonyl group of an asparagine and a backbone amide of asparagine 3 residues

940   earlier (highlighted in red) that are observed in [29]. (B) Electron density (blue mesh;

941     $2mF_o$-dF_c at 1 σ) of the 2A10 F_{AB} fragment viewed from above the antigen-binding

942   site. Light chain is shown as yellow sticks, heavy chain as cyan. (C) A calculated

943   model of the $(NANP)_6$:2A10 F_{AB} fragment complex. The CDR2 regions of each chain

944   are shown in red, the CDR3 regions of each chain are shown in blue.

945

946 **Fig 3. Detailed view of the $(NANP)_6$:2A10 F_{AB} interface and site directed**

947 **mutagenesis.** (A) A model of the light chain:$(NANP)_6$ interface. (B) ELISA results

948 showing the effect of mutating light chain interface residues; error bars are based on

949 technical replicates from one of two independent experiments. (C) A model of the

950 heavy chain:$(NANP)_6$ interface. (D) ELISA results showing the effect of mutating

951 heavy chain interface residues; error bars are based on technical replicates from one

952 of two independent experiments.

953 **Fig 4. The multivalency of the NANP repeat region of the CSP protein.** (A) An

954 $(NANP)_6$ peptide results in the presentation of two symmetrical epitopes, formed by

955 alternating repeats (cyan and magenta), allowing binding by two F_{AB} domains, in

956 keeping with the stoichiometry observed by ITC. (B) The full 27-mer repeat region

957 results in the presentation of at least 10 separate epitopes and the twist of the helix

958 results in displacement along the length of the repeat region, which allows binding of

959 up to 10 separate F_{AB} fragments, consistent with 4 antibodies bound by both F_{AB}

960 domains, and two bound by a single F_{AB} domain.

961

962 **Fig 5. CSP-specific B cells enter the germinal center following sporozoite**

963 **immunization.** BALB/C mice were immunized with either 5 x 10^4 *P. berghei* CS^{5M}

964 (expressing the endogenous *P. berghei* CSP repeat) or 5 x 10^4 *P. berghei* CS^{Pf}

965 (expressing the circumsporozoite protein from *P. falciparum*) live spoorzoites under

966 CQ cover. 12 days later the B cell response was analyzed by flow cytometry and

967 putative $(NANP)_n$-specific cells were identified using PE and APC conjugated

968 tetramers. (A) Representative flow cytometry plots showing the identification of

969     $(NANP)_n$-specific (Tetramer$^+$) cells. (B) Representative flow cytometry plots showing

970   the proportion of Tetramer$^+$ cells that have class switched and entered a GC. (C)

971   Quantification of the number of class switched Tetramer$^+$ cells under different

972   immunization conditions. (D) Quantification of the number of GC Tetramer$^+$ cells

973   under different immunization conditions. Data from a single representative

974   experiment of 2 repeats, analyzed by one-way ANOVA with Tukey's post test.

975

976   **Fig 6. The B cell response to CSP has a T-independent component.** CD28$^{-/-}$ and

977   control C57BL/6 mice were immunized with *P. berghei* CS^{Pf} radiation attenuated

978   sporozoites (RAS) or rCSP in alum. Sera were taken and the spleens analyzed for

979   antigen specific B cells using tetramers 4, 7 and 27 days post-immunization. (A) IgM

980   and IgG $(NANP)_n$ ELISA responses following RAS immunization (B) Representative

981   flow cytometry plots 7 days post RAS immunization showing the gating of different

982   B cell populations among Tetramer$^+$ cells. (C) Absolute numbers of (i) total Tetramer$^+$

983   IgD$^-$ve (ii) Tetramer$^+$ Plasmabalsts and (iii) Tetramer$^+$ GC B cells post RAS

984   immunization. (D) Antibody responses and (E) absolute numbers of Tetramer$^+$ IgD$^-$ B

985   cells 4 days post immunization with rCSP. Log-transformed data pooled from 2

986   independent experiments for each immunization (>3 mice/group/timepoint) were

987   analyzed using linear mixed models with day and genotype/immunization as

988   experimental factors and the individual experiment as a random factor; only

989   significant differences are shown.

990

991   **Fig 7. Limited diversity of $(NANP)_n$ specific antibodies.** BCR sequences were

992   amplified from Tetramer$^+$ cells sorted from BALB/C mice 35 days after immunization

993   with live *P. berghei* CS^{Pf} sporozoites under CQ cover as well as bulk (B220+) B cells

994   from naïve BALB/C mice (A) IGHV gene usage from among B cells from a

995   representative naïve mouse (grey bars) and Tetramer+ cells from immune mice (red,

996   blue and yellow bars). (B) Shannon's diversity calculated for the diversity of IGHV

997   region usage among bulk B cells and Tetramer$^+$ cells. (C) Circos plots showing the

998   IGHV-IGHJ pairings in a representative naïve mice and 3 immune mice. (D) IGKV

999   gene usage from among B cells from a representative naïve mouse (grey bars) and

1000   Tetramer+ cells from immune mice (red, blue and green bars). (E) Shannon's diversity

1001   calculated for the diversity of IGKV region usage among bulk B cells and Tetramer$^+$

1002   cells. (F) Circos plots showing the IGKV-IGKJ pairings in a representative naïve

1003   mouse and 3 immune mice. Statistical analysis of Shannon's diversity index was by

1004   Student's T test.

1005

1006   **Fig 8. CSP-binding antibodies undergo somatic hypermutation and affinity**
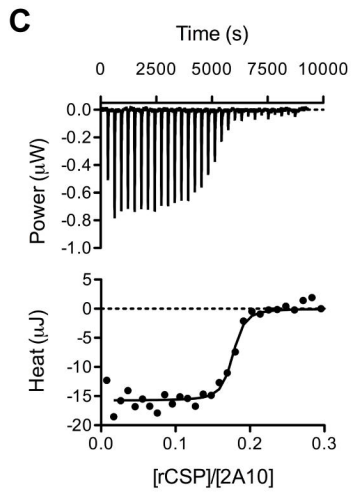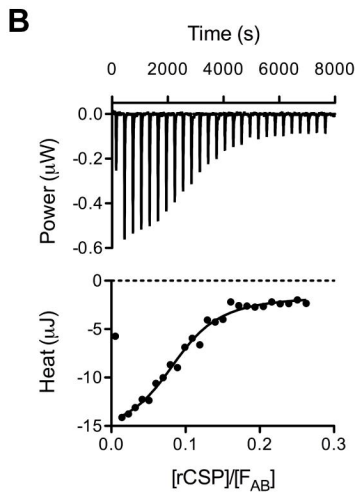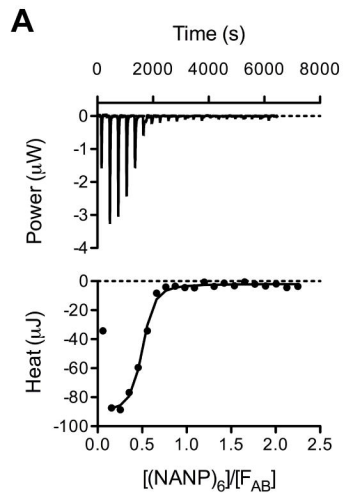
1007   **maturation** (A) Violin plots showing the number of mutations per kappa chain read

1008   from bulk B cells from 3 individual naïve mice and sorted $(NANP)_n$ specific B cells

1009   from sporozoite immunized mice (B) Skyscraper plots showing the location of

1010   mutations away from germline in the IGKV1-110 gene in a naïve mouse and in sorted

1011 $(NANP)_n$ specific cells in three sporozoite immunized mice. (C) ELISA binding to the

1012 $(NANP)_9$ peptide of recombinant antibodies corresponding to the 2A10 mAb, the

1013   predicted germline precursor, and hybrid antibodies containing the 2A10 heavy chain

1014   (mHC) paired with the germline light chain (gLC) and the 2010 light chain (mLC)

1015   paired with germline heavy chain (gHC). (D) Predicted mutations in the gLC were

1016   introduced to the germline precursor and their effect on binding to $(NANP)_9$ measured

1017   by ELISA (E) Predicted mutations in the gHC were introduced to hybrid antibodies

1018   consisting of the mLC and the gHC heavy chain and their effect on binding to

1019   (NANP)$_9$ measured by ELISA.

1020

1021

A

Time (s)

B

Time (s)

C

Time (s)

A

Y56
Y38
R109
Y116
S36

B Light Chain Mutations

S36A
mAb
R109A
Y116F
Y56A
Y38A

(NANP)$_9$ binding (Abs$_{405}$)

[Antibody] (µg/ml)

C

E64
T66
N57
Y37
Y56

D Heavy Chain Mutations

E64A
mAb
T66A
Y37A
N57A

(NANP)$_9$ binding (Abs$_{405}$)

[Antibody] (µg/ml)

A Gated on B cells

Naïve | *P. berghei* CS^5M | *P. berghei* CS^Pf

0.032% | 0.031% | 0.27%

Tet+ cells

Tet-PE (y-axis) / Tet-APC (x-axis)

B Gated on Tet+ B cells

Naïve | *P. berghei* CS^5M | *P. berghei* CS^Pf

Switched cells

1.35% | 4.67% | 82.0%

IgM (y-axis) / IgD (x-axis)

GC B cells

0% | 1.34% | 55.4%

CD38 (y-axis) / GL7 (x-axis)

C

Switched Tet+ cells/10^6 B cells

**** | ****
ns

Naïve | *P. berghei* CS^5M | *P. berghei* CS^Pf

D

GC Tet+ cells/10^6 B cells

**** | ****
ns

Naïve | *P. berghei* CS^5M | *P. berghei* CS^Pf

A

i RAS: IgM

WT / CD28$^{-/-}$

(NANP)$_9$ ELISA binding (AUC), y-axis

Day 4, 7, 27; ** at day 7; * at day 27

ii RAS: IgG

(NANP)$_9$ ELISA binding (AUC), y-axis

Day 4, 7, 27; * at day 7; *** at day 27

B

Tetramer+ B cells / IgD- Tet+ cells / Non-PB

naïve (WT): IgD-Tet+ 28.8%; PB 5.26%; GC B cells 0%

immune: d7 (WT): 75.6%; 7.69%; 45.5%

immune: d7 (CD28$^{-/-}$): 37.1%; 9.57%; 10.9%

Axes: IgM vs IgD; FSC vs CD138; CD38 vs GL7

C i RAS: IgD- Tet+ cells

IgD- Tet+ cells/spleen, y-axis

Day 4, 7, 27; naïve / WT / CD28$^{-/-}$

ii RAS: Plasmablasts

Tet+ PBs/spleen, y-axis

Day 4, 7, 27

iii RAS: GC B cells

Tet+ GC B cells/spleen, y-axis

Day 4, 7, 27

D i rCSP: IgM

(NANP)$_9$ ELISA binding (AUC); WT vs CD28$^{-/-}$

ii rCSP: IgG

(NANP)$_9$ ELISA binding (AUC); WT vs CD28$^{-/-}$; *

E rCSP: IgD- Tet+ cells

IgD- Tet+ cells/spleen; naïve / WT / CD28$^{-/-}$; **

A

B

Naïve B cells
CDR1   CDR2   CDR3

Immune 1

Immune 2

Immune 4

Mutation to:
G
T
C
A

Nucleotide position

C
mAb
gHCmLC
mHCgLC
gAb

D
Light chain SHM
gHCmLC
68Y;114F;117V
114F;117V
L114F
T117V
H68Y
gAb
S66T

E
Heavy chain SHM
mAb
M39I
N59I
T67F
gHCmLC

(NANP)9 binding (Abs405)

[Antibody] (µg/ml)